Catalysis Today 146 (2009) 9–14

Contents lists available at ScienceDirect

Catalysis Today

journal homepage: www.elsevier.com/locate/cattod

Carbon-supported PtNi catalysts for electrooxidation of cyclohexane to benzene over polymer electrolyte fuel cells

Hyung Ju Kim, Sung Mook Choi, Sang Hoon Nam, Min Ho Seo, Won Bae Kim *

Department of Materials Science and Engineering, Gwangju Institute of Science and Technology (GIST), 261 Cheomdan-gwagiro, Gwangju 500-712, South Korea

ARTICLE INFO

Article history:
Available online 3 January 2009

Keywords:
PtNi catalyst
Cyclohexane oxidation
Fuel cells
Cyclic hydrocarbons
Benzene

ABSTRACT

Electrochemical dehydrogenative oxidation of cyclohexane to benzene was studied over carbon-supported PtNi (PtNi/C) electrocatalysts, which were prepared using a borohydride reduction method combined with a freeze–drying procedure at room temperature. The carbon-supported bimetallic PtNi catalysts were characterized by various physicochemical analyses such as X-ray diffraction (XRD), transmission electron microscopy (TEM), energy dispersive X-ray spectroscopy (EDS), extended X-ray absorption fine structure (EXAFS) and X-ray absorption-near-edge spectroscopy (XANES). The addition of Ni content to the Pt-based catalysts caused structural and electronic modifications over the PtNi alloy catalyst formation, which could directly affect the electrocatalytic activity of cyclohexane oxidation. The Pt_1Ni_1/C catalyst as an anode electrocatalyst showed a maximum power density of *ca.* 30 mW cm^{-2} mg_{Pt}^{-1}, which is 2 times or greater power density than that of Pt/C per Pt milligram. Here, both the structural modification via Pt–Pt bond distance change and the electronic modification through charge transfer from Ni to Pt should be responsible for the activity enhancement in the PtNi/C by facilitating the dehydrogenative electrooxidation of cyclohexane to benzene over the PtNi/C anode of cyclohexane-fueled fuel cell system.

1. Introduction

A fuel cell is an efficient energy conversion system and provides many advantages like zero or low emission of pollutants and high efficiency [1–3]. Among several kinds of fuel cells, polymer electrolyte membrane fuel cell (PEMFC) using hydrogen gas as a fuel has received considerable attention for transportation and portable applications due to its high power density, relatively low operating temperature and least emission of pollutants except water during the operation [4]. However, transportation and storage of the hydrogen gas remain to be still an important technical barrier [5]. As the other type of PEMFCs, direct methanol fuel cell (DMFC) has been developed as a promising alternative power source for portable electronic devices because the methanol itself is an abundant and inexpensive liquid fuel that can be easily stored and transported [6–9]. Moreover, the DMFC has high energy capacity for the portable applications, but it has been still suffered from several technical issues [10,11].

Recently, new types of polymer electrolyte fuel cells operating with cyclohexane [12,13], propane [14], butane or ethane [15] as fuel have been tried. Among these fuels, cyclohexane would be one of the promising fuels because it is easy to handle, store and transport with relatively high energy contents [16,17]. More importantly, cyclohexane can take advantage of reversible catalytic processes of dehydrogenation reaction of cyclohexane to benzene and hydrogenation reaction of benzene to cyclohexane. The dehydrogenative electrooxidation of cyclohexane to benzene can generate electric power without emissions of CO and CO_2 with negligible fuel crossover of cyclohexane [12,13]. Therefore, the cyclohexane-fueled polymer electrolyte membrane (PEM) type fuel cell may be potentially implicated as the low or mediocre power sources against the disadvantages of DMFCs such as catalyst poisoning by CO and methanol crossover across the PEM [18,19].

The performances of PEM fuel cell operating with cyclohexane were studied and compared using the commercial carbon-supported Pt and Pt-based electrocatalysts such as PtRu, PtPd, PtRh as the anode catalysts in the previous literature reported by Kariya et al. [12], in which the PtRh catalyst showed the best performance. Using the PtRh/C catalyst system, we also have studied the Rh effect on the dehydrogenative electrooxidation of cyclohexane to benzene over a polymer electrolyte membrane fuel cell [20], in which the variation of Rh content over PtRh alloy catalyst formation caused significant structural and electronic modifications on the catalyst phase, leading to consistent changes in electrocatalytic activities determined through electrochemical current–voltage (*I–V*) measurements. However, both precious metals of Pt and Rh are very expensive; the Rh is even much more

* Corresponding author. Tel.: +82 62 970 2317; fax: +82 62 970 2304.
E-mail address: wbkim@gist.ac.kr (W.B. Kim).

0920-5861/$ – see front matter © 2008 Elsevier B.V. All rights reserved.
doi:10.1016/j.cattod.2008.11.012

expensive than Pt, thus many efforts to replace with non-precious metal catalysts or to reduce the use of platinum have been devoted.

In this study, we investigate carbon-supported bimetallic PtNi (PtNi/C) catalyst on their structural, electronic and electrochemical features for the electrooxidation of cyclohexane over the PEM type fuel cell. The catalyst is characterized by employing various physicochemical analyses such as X-ray diffraction (XRD), transmission electron microscopy (TEM) and extended X-ray absorption fine structure (EXAFS) to investigate the structural modification, energy dispersive X-ray spectroscopy (EDS) to obtain the information on the chemical property, and X-ray absorption-near-edge spectroscopy (XANES) to characterize the electronic features. Based on their physicochemical properties, electrocatalytic activities will be explored and discussed with addition of Ni content for the dehydrogenative electrooxidation of cyclohexane to benzene over the PtNi/C anode catalyst in the polymer electrolyte membrane fuel cell.

2. Experimental

2.1. Synthesis of carbon-supported bimetallic PtNi catalyst

The carbon-supported 40 wt.% bimetallic PtNi catalysts (Pt:Ni = 2:1, 1:1 with 40 wt.% metal loading) were synthesized through conventional borohydride reduction method using $NaBH_4$ (Aldrich) solution combined with freeze–drying procedure. Carbon support used in this study was Vulcan XC-72R (Cabot Corp., S_{BET} = 236.8 $m^2\ g^{-1}$). Pt salt ($H_2PtCl_6{\cdot}xH_2O$, Aldrich) and Ni salt ($NiCl_2{\cdot}6H_2O$, Aldrich) were used as the precursors for the PtNi catalysts. For a typical synthesis, a pre-measured amount of the carbon support was dispersed in a triply de-ionized (DI) Millipore water (18 MΩ cm) while stirring with sonication for a few hours. Calculated amounts of Pt and Ni salt were mixed in the de-ionized Millipore water until they were completely dissolved under sonication. The precursor solutions and carbon were mixed in the DI water and stirred for several hours. The catalyst precursors were then reduced by drop-wise addition of a freshly prepared 0.1 M aqueous $NaBH_4$ solution (Aldrich) using a syringe pump (KD Scientific Inc.). The solid parts were filtered and washed several times with the DI water, and subsequently vacuum dried at −80 °C via a freeze–drying method for highly dispersed nanoparticle catalysts by minimizing particle agglomeration.

2.2. Characterizations of the PtNi/C catalyst

The crystalline characteristics of the carbon-supported Pt and PtNi catalysts were examined by powder X-ray diffraction technique using a Rigaku Rotalflex (RU-200B) X-ray diffractometer with a Cu Kα (λ = 1.5405 Å) source and a Ni filter, which allows one to confirm alloy formation and characterize structural evolution of the PtNi crystallite with addition of Ni content. The source was operated at 40 kV and 40 mA, and the 2θ angular region between 10° and 80° was explored at a scan rate of 3° min^{-1}.

The morphologies of Pt and PtNi nanoparticles on the carbon support were investigated using a JEOL JEM-2100 transmission electron microscope operated at 200 kV. All TEM samples were prepared by ultrasonically suspending the catalyst particles in an ethanol solution. Drops of the suspension were deposited onto a standard Cu grid (200-mesh) covered with a carbon film and dried for 20 min to allow ethanol and water to be evaporated, leaving the catalyst particles dispersed on the grid prior to being inserted into the microscope. The energy dispersive X-ray spectroscopy analysis was performed at 200 kV using an INCA-X, Oxford attached to the TEM.

X-ray absorption measurements were conducted on 3C1 and 7C beamlines of Pohang Accelerator Laboratory (PAL; 2.5 GeV with the stored currents of 130–180 mA) in Korea. A Si (1 1 1) double crystal monochromator was employed to monochromatize the X-ray photon energy. The incident beam intensity was monitored using an ionization chamber purged with a gas mixture of N_2 (80%) and Ar (20%), and the transmitted beam intensity was measured in an ionization chamber filled with a pure N_2 flow. The spectra were taken at room temperature in a transmission mode for L_3-edge of Pt (11564 eV) under the ambient condition. Higher order harmonic contamination was eliminated by detuning the monochromator to reduce the incident X-ray intensity by about 30%. Energy calibration was performed using a standard Pt metal foil. The X-ray absorption-near-edge spectra were analyzed using the IFEFFIT software programs [21,22]. The pre-edge background was removed in a pre-edge region of 11,414–11,514 eV with a straight line and the extrapolated values were subtracted from the entire spectrum. The resulting elemental absorption was then normalized by using atomic-like absorption at the edge. The white line (WL) areas of Pt L_3-edge were calculated by adopting an arctangent step and by fitting a Lorentzian function to the WL curve in the region from −50 to 100 eV around the edge energy. The extended X-ray absorption fine structure (EXAFS) data for the PtNi/C catalyst were analyzed using the IFEFFIT software programs [21,22] and the FEFF 8.4 code [23]. The interference function of the EXAFS data is defined as $\chi(E) = (\mu(E) - \mu_0(E))/\Delta\mu_0(E_0)$ above the absorption edge E_0, where $\mu(E)$ is the absorption coefficient due to the particular edge of the element in sample, $\mu_0(E_0)$ is the atomic-like absorption, and $\Delta\mu_0(E_0)$ is the jump at the edge step. The post-edge background function $\mu_0(E)$ is approximated by a piecewise spline that can be adjusted so that low-R components of the Fourier-transformed data $\chi(R)$ are optimized. The power-scale EXAFS function $k^3\chi(k)$ in the momentum k space was Fourier-transformed to obtain the radial structural function (RSF) of the samples [24]. The number of parameters we can reliably measure is limited as following equation:

$$N \approx \frac{2\,\Delta k\,\Delta R}{\pi},$$

where Δk and ΔR are the k- and R-ranges of the usable data.

2.3. MEA fabrication and single cell test

Membrane electrode assemblies (MEAs) were fabricated by sandwitching 40 wt.% Pt/C (E-Tek) as the cathode electrode, Nafion® 117 (DuPont) as the PEM, and the home-made PtNi/C catalyst as the anode electrode. Each catalyst slurry was made of catalyst, Nafion ionomer solution (5 wt.%, DuPont), and isopropyl alcohol. The ratio of catalyst and Nafion solution was controlled to be 85 wt.%:15 wt.% for all cases. The slurries were sonicated and stirred for 3 h to disperse the catalyst. The amount of loaded metal in electrodes was fixed to be 1 $mg_{metal}\ cm^{-2}$ in all cases. The PEM of Nafion® 117 had been treated in 5% H_2O_2 solution for 1 h at 80 °C and washed with DI water, followed by treatment in 1 M H_2SO_4 solution for 1 h at 80 °C with subsequent washing by DI water. After the pretreatments of PEM membranes, they were dried and kept compressed before MEAs fabrication that was done by hot-pressing the Nafion membrane with anode and cathode electrodes at 120 °C under 35 MPa for 4 min.

Electrocatalytic activities of cyclohexane oxidations were measured at an operating temperature of 100 °C over a single cell jacketed with 4 cm^2 gold-plated (1 μm Au thickness) SUS 304 punched sheets as the current collector. Considering the structure of current collector, the geometric area for the cyclohexane oxidation reaction would be 2.89 cm^2. Fig. 1 illustrates the experimental system set-up used in this work, in which the liquid cyclohexane (99.5%, Kanto Chemical Co. Inc.) was injected at a feeding rate of 15.0 ml h^{-1} and evaporated under a dinitrogen

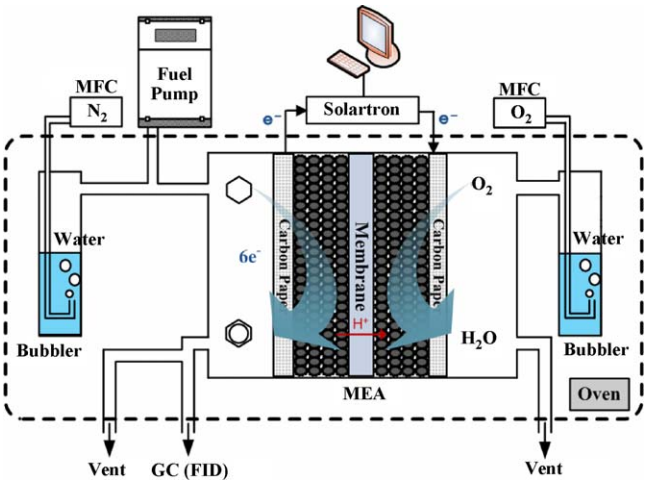

Fig. 1. Schematic illustration of single cell tests employed here for the electrooxidation of cyclohexane to benzene over the polymer electrolyte membrane fuel cell.

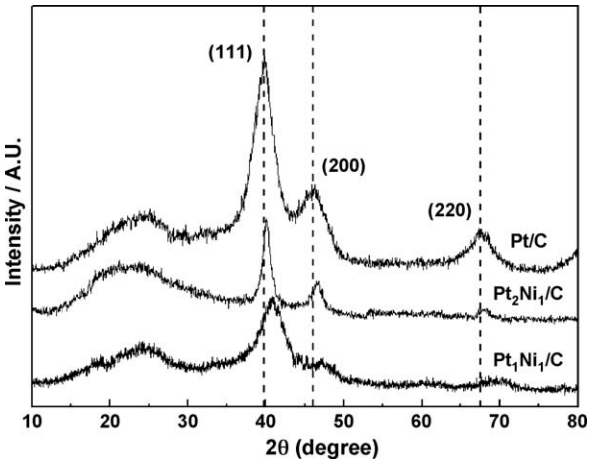

Fig. 2. X-ray diffraction patterns of the commercial 40 wt.% Pt/C (E-Tek) and prepared 40 wt.% PtNi/C catalysts over the scan range of 10–80°. The dashed lines indicate the typical diffraction angles of the *fcc* phase of Pt.

carrier gas at 100 ml min^{-1} that was pre-saturated with water vapour in an oven at 100 °C. O_2 gas was fed at 100 ml min^{-1} into the cathode. The outstream product gas from the working anode that contains unreacted cyclohexane and produced benzene was timely analyzed by using the flame ionization detector (FID) of gas chromatography (GC), along with electrochemical current–voltage (*I–V*) measurements. An HP 5890 series II GC equipped with an EC^{TM}-WAX (stationary phase) capillary column (Alltech) was employed for the gas composition analysis. *I–V* measurements were performed by a galvanodynamic method using an electrochemical cell test system (Solartron 1400). Potentials were scanned to the anodic direction at a scan rate of 0.3 mA s^{-1} for the polarization measurements in the potential range of 0–1000 mV.

3. Results and discussion

3.1. Structural and chemical analysis of PtNi/C catalyst

Fig. 2 shows XRD patterns of the carbon-supported 40 wt.% Pt (a commercial catalyst purchased from E-Tek) and home-made PtNi catalysts, in which the characteristic peaks from a crystalline face centered cubic (*fcc*) Pt phase appear at the corresponding diffraction angles for the (1 1 1), (2 0 0) and (2 2 0) planes. The typical *fcc*-Pt diffraction peaks in the PtNi/C catalysts seem to be broadened and there are no noticeable peaks for phase separated structures such as a pure Ni or its oxides in our XRD measurements, indicating a good degree of alloying between Pt and Ni. In particular, the diffraction peaks were slightly shifted to the higher 2θ values in the PtNi/C catalysts as compared to those of the Pt/C; such shifts could be an evidence for the alloy formation between Pt and Ni [25,26]. The average particle sizes and lattice parameters for the single-phase Pt in Pt/C or bimetallic PtNi (solid solution) in PtNi/C catalysts were evaluated using the full width at half maximum (FWHM) and the angular position ($2\theta_{max}$) of the (2 2 0) peaks [27], as summarized in Table 1. The lattice parameter values appeared to be decreased from Pt/C to Pt_1Ni_1/C catalysts with Ni content, indicating that lattice contractions occurred due to partial substitution of Pt by Ni [25,26].

The morphology and particle size distribution of the catalysts were observed by TEM in Fig. 3. The average size of PtNi nanoparticles in the PtNi/C catalysts was about 2.5 nm with a standard deviation of 0.5 nm, which was estimated by averaging diameters of at least 100 different nanoparticles seen in the magnified TEM photograph. The TEM-measured particle sizes of the PtNi are a little bit smaller than that of Pt/C (*ca.* 2.7 nm), as summarized in Table 1. The purity and chemical composition of the nanoparticles, especially of the Pt_1Ni_1, could be investigated by point-resolved EDS analysis in Fig. 4, indicating an atomic composition of approximately 50:50 of Pt:Ni. All of the XRD, TEM and EDS results complementarily indicate that the synthesized nanoparticles in the PtNi alloy phase are highly dispersed on the carbon support, demonstrating that the borohydride reduction method combined with the freeze–drying procedure in this work would be an effective method to prepare nanosized bimetallic PtNi system. There appeared no significant difference in the metal particle size with addition of Ni content under our preparation condition from the commercial Pt/C, allowing particle size effect to be excluded from the influential parameters for the electrocatalytic activity over the carbon-supported PtNi catalyst.

Table 1
Structural and electronic parameters of the PtNi/C catalysts characterized by XRD, TEM and XANES analyses.

Catalysts	$2\theta_{max}$[a] (°)	Lattice parameter[b] (Pt–Pt bond distance) (Å)	Mean particle size (nm)		XANES parameters	
			XRD[c]	TEM[d]	E_0[e] (eV)	WL intensity[f] (a.u.)
Pt/C	67.70	3.911 (2.765)	3.0	2.7 ± 0.5	11567.9	1.32
Pt_2Ni_1/C	68.33	3.880 (2.744)	2.8	2.5 ± 0.5	–	–
Pt_1Ni_1/C	69.72	3.812 (2.695)	2.5	2.5 ± 0.6	11567.5	1.28

[a] The angular position of Pt (2 2 0) reflection peak.
[b] Lattice parameter and Pt–Pt bond distance calculated from XRD measurement.
[c] Mean particle diameter of the metal catalyst calculated by line broadening of powder. XRD peak using the Scherrer equation.
[d] Mean particle diameter of the metal catalyst from TEM images using at least 100 visible particles.
[e] Pt L_3-edge energy.
[f] White line intensity.

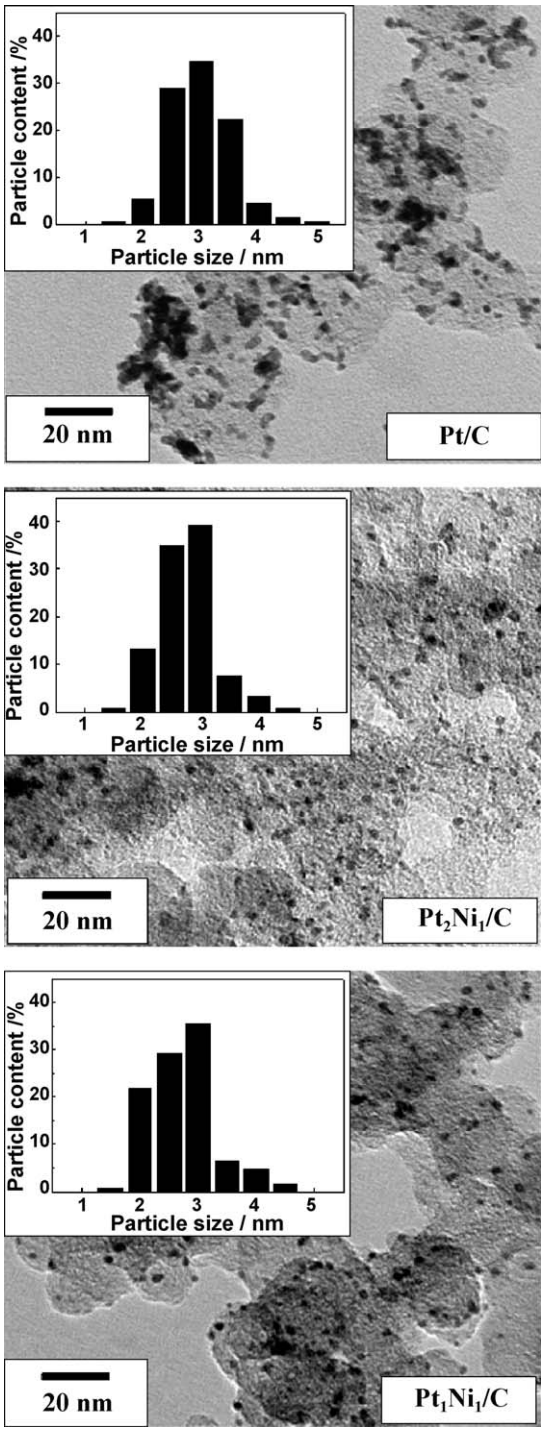

Fig. 3. Representative TEM images of the carbon-supported 40 wt.% Pt (E-Tek) and PtNi catalysts, together with particle-size distributions of the metal nanoparticles.

Fig. 5 shows Fourier transformed (FT) EXAFS profiles of the Pt/C and PtNi/C catalysts together with the Pt foil reference for the Pt–Pt bond. These FT-EXAFS data are characterized by a main peak located at a radial distance of *ca.* 2.75 Å, which is likely due to the phase-uncorrected first shell of Pt–Pt interaction [28,29] for the single component of Pt/C and the interfered interactions of Pt–Pt with Pt–Ni bonds for the alloyed PtNi/C system. In order to obtain quantitative information on the coordination number (CN) and radial distance of the local environment of Pt, we fitted the experimentally derived radial structural function with theoretical Pt–Pt and Pt–Ni scatterings. The fitting results are summarized in

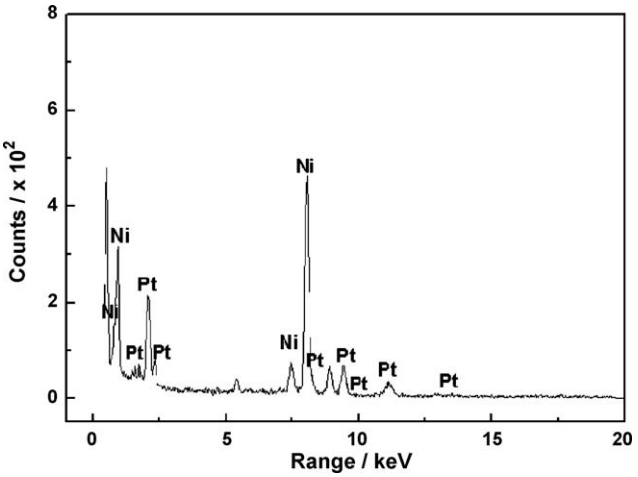

Fig. 4. EDS spectra for the prepared Pt_1Ni_1/C catalyst.

Table 2. The CN of the commercial Pt/C catalyst showed about 8.83, which is definitely smaller than the theoretical CN value of 12 for the bulk *fcc* crystallite like Pt foil because of its nanosize feature with an average diameter of *ca.* 2.7 nm from the TEM observation. For the alloyed PtNi catalyst, the total CN contributed by both Pt–Pt and Pt–Ni interactions was about 7.0. The Pt–Pt bond distance in case of PtNi/C catalyst showed a decreased propensity than that of Pt/C, which is in line with the previous literatures [30,31]. Also, the Pt–Pt bond distances determined from XRD (Table 1) and EXAFS (Table 2) analysis exhibited a good agreement.

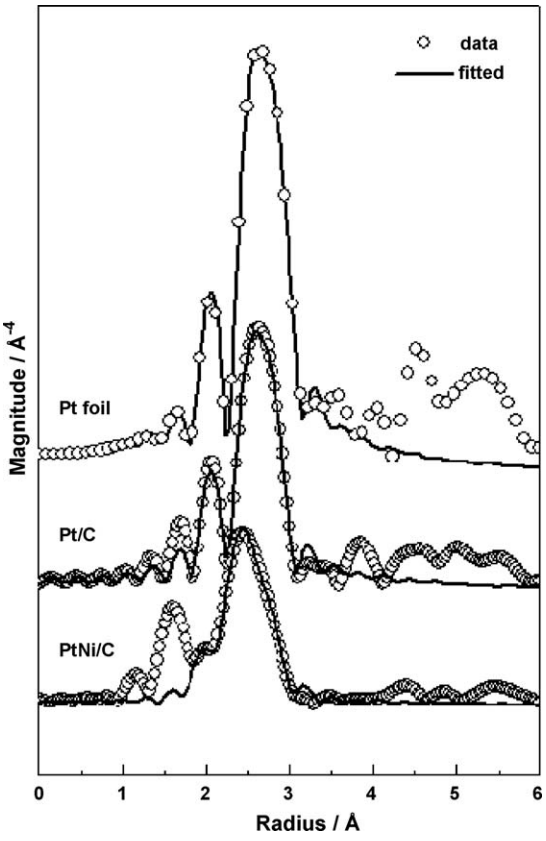

Fig. 5. FT-EXAFS profiles for the Pt foil, Pt/C, and PtNi/C catalyst with the sample spectra (–) and their fitted functions (○).

Table 2
EXAFS fitting results for the first shell of Pt/C and PtNi/C catalyst.

Catalyst	Pt–Pt interaction		Pt–Ni interaction	
	CN[a] (±1)	R[b] (±0.01 Å)	CN[a] (±0.1)	R[b] (±0.01 Å)
Pt foil	12	2.767	–	–
Pt/C	8.83	2.748	–	–
Pt_1Ni_1/C	6.36	2.700	0.64	2.730

[a] The average coordination number for the coordination shell.
[b] Inter-atomic distance; the theoretical values of Pt–Pt and Pt–Ni distance are 2.772 and 2.772 Å, respectively.

3.2. Electronic structure of PtNi/C catalyst

The electronic structure of platinum in the prepared PtNi/C electrocatalyst was investigated by Pt L_3-edge XANES as shown in Fig. 6. The absorption jump at the Pt L_3-edge (*ca.* 11564 eV) corresponds to $2p_{3/2} \rightarrow 5d$ electronic transitions [28,32]. The overall XANES shapes for the bimetallic PtNi/C are similar to those of the Pt foil and Pt/C except the edge absorption intensity. The strong peak above the edge energy position (see the magnified region in the inset figure) is closely associated with the density of vacant 5d electronic states of Pt [32]; this is called the white line peak and is frequently recognized as an important parameter in catalytic activity [28]. The WL magnitudes were smaller in the bimetallic PtNi/C catalyst than that of Pt/C catalyst. Note that the average particle sizes are almost same in both catalyst systems of Pt/C and PtNi/C. Therefore, this decreased WL intensity should be attributed to partial filling of the unoccupied Pt 5d orbital in the PtNi alloy by electrons that are donated from adjacent Ni, showing an agreement with the XPS study on PtNi catalyst [25], which can be also interpreted from the electronegativity difference of Ni and Pt element with 1.91 and 2.28, respectively, thereby the electronic transition of $2p \rightarrow 5d$ is suppressed. These analyses of electronic structures through Pt L_3-edge XANES investigation were included in Table 1 for the quantitative WL values together with the edge energy analysis.

3.3. Cyclohexane fuel cell performance with PtNi/C anode catalyst

Fig. 7 shows the performance of fuel cells that are fueled with cyclohexane over the commercial 40 wt.% Pt/C (E-Tek) and home-made 40 wt.% PtNi/C catalysts as the anode catalyst. The 40 wt.% Pt/C (E-Tek) was used as the cathode catalysts for all performance measurements. The catalyst loading of all anode and cathode

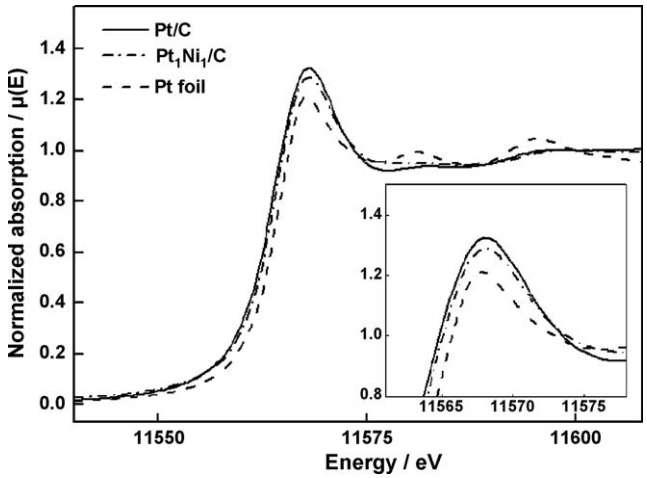

Fig. 6. Pt L_3-edge XANES spectra for the Pt/C (E-tek) and home-made PtNi/C catalyst together with Pt foil as the reference.

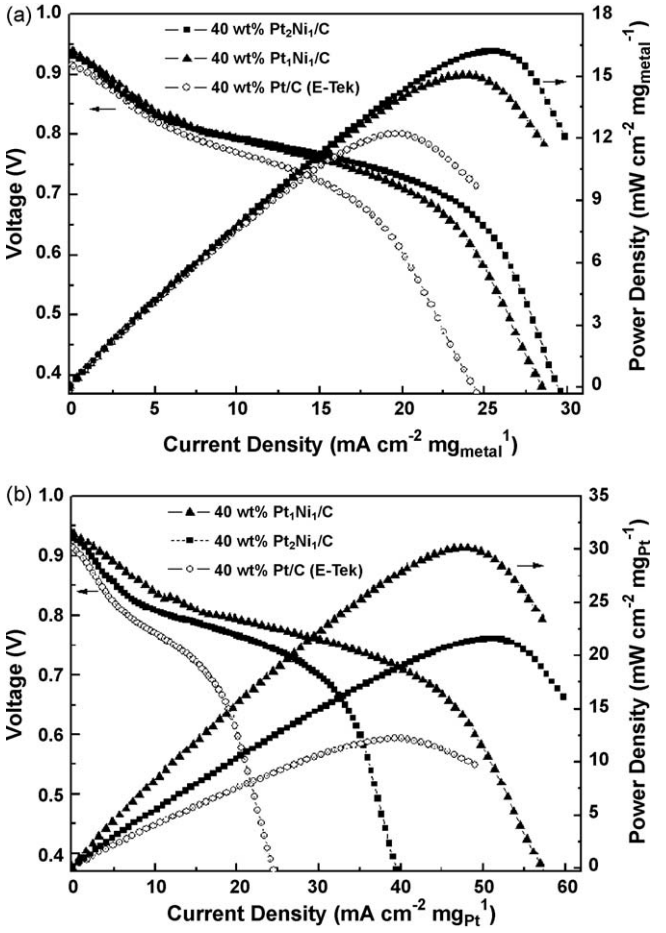

Fig. 7. *I–V–P* curves per metal milligram (a) and Pt milligram (b) for the dehydrogenative eletrooxidation of cyclohexane to benzene over the commercial 40 wt.% Pt/C (E-Tek) and home-made 40 wt.% PtNi/C catalysts as the anode of polymer electrolyte membrane fuel cell at 100 °C.

electrodes was fixed to *ca.* 1 mg of metal per unit cm^2 of electrode area. The fuel cell operating temperature was 100 °C with a cyclohexane fuel feeding rate of 15 ml h^{-1}. It is worthwhile to note that the cyclohexane fuel generates a relatively high open circuit voltage (OCV) as high as 0.938 V even at 100 °C in our system, while non-electrochemical catalytic dehydrogenation of cyclohexane requires reaction temperatures above 250 °C [16,17], or direct propane/oxygen fuel cell needs reaction temperatures higher than 200 °C with 0.8 V of OCV [14]. If other hydrocarbon fuel cells using propane [14], butane or ethane [15] as the fuel are compared, the cyclohexane fuel cell may be supposed to outperform because of such a high value of OCV. In Fig. 7, current vs. voltage (*I–V*) curves are compared for the anode catalysts of Pt/C and PtNi/C, showing that the PtNi/C catalysts performs better with maximum power

Table 3
Electrochemical properties for the electrooxidation of cyclohexane to benzene of the commercial 40 wt.% Pt/C (E-Tek) and home-made PtNi/C catalysts over the anode of polymer electrolyte membrane fuel cell at 100 °C.

Catalyst	OCV[a] (mV)	Max.P.D.[b] ($mW\ cm^{-2}\ mg_{metal}^{-1}$)	Max.P.D.[c] ($mW\ cm^{-2}\ mg_{Pt}^{-1}$)
Pt/C	915	12.1	12.1
Pt_2Ni_1/C	932	16.2	21.6
Pt_1Ni_1/C	938	15.1	30.1

[a] Open circuit voltage.
[b] Maximum power density per metal milligram.
[c] Maximum power density per Pt milligram.

densities of *ca*. 15.1 and 16.2 mW cm^{-2} $mg_{metal}{}^{-1}$, for the Pt_1Ni_1/C and Pt_2Ni_1/C, respectively, than that of the commercial Pt/C showing *ca*. 12.0 mW cm^{-2} $mg_{metal}{}^{-1}$ for the dehydrogenative electrooxidation of cyclohexane. More interestingly, when the maximum power densities are normalized by miligram of Pt, 2 times or greater activity can be observed in case of the Pt_1Ni_1/C catalyst than Pt/C. Table 3 summarizes the OCV and power density values of the cyclohexane electrooxidation to benzene over the Pt/C and PtNi/C catalysts. For the product analysis, outlet gases exhausted from the anode chamber during the electrooxidation reaction were analyzed by gas chromatography, but we could not observe any intermediates or by-products except the reactant of cyclohexane and the product of benzene from the anode gases, which agrees to the previous literature [12,13].

The XRD and EXAFS analyses, as shown in Figs. 2 and 5 and as summarized in Tables 1 and 2, indicated that the geometric environment of the PtNi/C catalyst was changed by forming solid solutions of PtNi alloy phase, accompanying a decrease in Pt–Pt bond distance as compared to that of pure Pt. There have been several reports that the catalytic activity is affected by Pt–Pt bond distance for the electrochemical oxidations of simple alcohols [33] and for the oxygen reduction reaction [4,30,34]. Therefore, structural change by adding Ni to Pt might play roles for the catalytic activity by modifying adsorption ability of cyclohexane on Pt surfaces. Also, the electronic structure modification can be responsible for the improved activity over the bimetallic PtNi system since the noticeable change with Ni incorporation in the charge transfer from Ni atoms to neighboring Pt atoms could be seen from the white line intensities in XANES (see Fig. 5 and Table 1). The electronic modification in the unfilled d band states of Pt atoms on the PtNi/C catalyst probably affects the C–H bond dissociation in the cyclohexane molecules, the adsorption/desorption properties of benzene and cyclohexane, and the easy formation of molecular hydrogen [35–37]. As a consequence of the Ni incorporation to the PtNi/C, the modified lattice parameter might favor the reaction *structurally* and the electronic modification with filling d band states of Pt atoms would promote the reaction *electronically*, both leading to enhancing the electrochemical catalytic activity over the dehydrogenative electrooxidation reaction of cyclohexane to benzene.

4. Conclusion

Electrochemical oxidative dehydrogenation of cyclohexane to benzene was studied over the commercial Pt/C (E-Tek) and home-made PtNi/C catalysts. The PtNi/C elelctrocatalysts showed the higher catalytic activity than the commercial Pt/C catalyst as the anode, resulting in the good performances in the voltage vs. current (*I*–*V*) curves with the greater power density. As the consequence of the Ni incorporation, the modifications of structural, electronic and electrochemical features on the PtNi/C catalyst were observed such as change in lattice parameter, charge transfer from Ni to Pt by partially filling of the Pt d-band vacancies, leading to modifying electrochemical catalytic activity on the dehydrogenative electrooxidation reaction of cyclohexane to benzene over the anode of a cyclohexane fuel cell.

Acknowledgements

This work was supported by New & Renewable Energy R&D program (2005-N-FC03-P-01-0-000) under the Korea Ministry of Commerce, Industry and Energy (MOCIE), and the Korea Research Foundation Grant of the Korean Government (MOEHRD) (KRF-2007-313-D00148). We also thank Dr. S.H. Choi and Dr. N.E. Sung at the Pohang Accelerator Laboratory in Korea for their helps and valuable discussions on the X-ray absorption experiments.

References

[1] B.B. McNicol, D.A.J. Rand, M.R. Williams, J. Power Sources 83 (1999) 15.
[2] M. Baldauf, W. Preidel, J. Power Sources 84 (1999) 161.
[3] G. Sattler, J. Power Sources 86 (2000) 61.
[4] J.R.C. Salgado, E. Antolini, E.R. Gonzalez, J. Power Sources 138 (2004) 56.
[5] R.F. Service, Science 285 (1999) 682.
[6] M. Hepel, I. Dela, T. Hepel, J. Luo, C.J. Zhong, Electrochim. Acta 52 (2007) 5529.
[7] X. Teng, X. Liang, S. Rahman, H. Yang, Adv. Mater. 17 (2005) 2237.
[8] J.S. Yu, S. Kang, S.B. Yoon, G. Chai, J. Am. Chem. Soc. 124 (2002) 9382.
[9] L. Cao, F. Scheiba, C. Roth, F. Schweiger, C. Cremers, U. Stimming, H. Fuess, L. Chen, W. Zhu, X. Qiu, Angew. Chem. Int. Ed. 45 (2006) 5315.
[10] Y. Paik, S.-S. Kim, O.H. Han, Angew. Chem. Int. Ed. 47 (2008) 94.
[11] Z. Wen, J. Liu, J. Li, Adv. Mater. 20 (2008) 743.
[12] N. Kariya, A. Fukuoka, M. Ichikawa, Chem. Commun. (2003) 690.
[13] N. Kariya, A. Fukuoka, M. Ichikawa, Phys. Chem. Chem. Phys. 8 (2006) 1724.
[14] C.K. Cheng, J.L. Luo, K.T. Chuang, A.R. Sanger, J. Phys. Chem. B 109 (2005) 13036.
[15] W.S. Li, D.S. Lu, J.L. Luo, K.T. Chuang, J. Power Sources 145 (2005) 376.
[16] N. Kariya, A. Fukuoka, M. Ichikawa, Appl. Catal. A 233 (2002) 91.
[17] N. Kariya, A. Fukuoka, T. Utagawa, M. Sakuramoto, Y. Goto, M. Ichikawa, Appl. Catal. A 247 (2003) 247.
[18] W. Yuan, K. Scott, H. Cheng, J. Power Sources 163 (2006) 323.
[19] M.H. Shao, K. Sasaki, R.R. Adzic, J. Am. Chem. Soc. 128 (2006) 3526.
[20] H.J. Kim, S.M. Choi, S.H. Nam, M.H. Seo, W.B. Kim, Appl. Catal. A 352 (2009) 145.
[21] M.J. Newville, J. Synchrotron Radiat. 8 (2001) 322.
[22] B. Ravel, M. Newville, J. Synchrotron Radiat. 12 (2005) 537.
[23] A.L. Ankudinov, A.I. Nesvizhskii, J.J. Rehr, Phys. Rev. B 67 (2003) 115120.
[24] B.K. Teo, EXAFS: Basic Principles and Data Analysis, Springer–Verlag, Berlin, 1986.
[25] K.-W. Park, J.-H. Choi, B.-K. Kwon, S.-A. Lee, Y.-E. Sung, H.-Y. Ha, S.-A. Hong, H. Kim, A. Wieckowski, J. Phys. Chem. B 106 (2002) 1869.
[26] S.-A. Lee, K.-W. Park, J.-H. Choi, B.-K. Kwon, Y.-E. Sung, J. Electrochem. Soc. 149 (2002) A1299.
[27] V. Radmilović, H.A. Gasteiger, P.N. Ross Jr, J. Catal. 154 (1995) 98.
[28] W. Vielstich, A. Lamm, H.A. Gasteiger, Handbook of Fuel Cells, vol. 2, John Wiley & Sons, England, 2003, p. 279.
[29] A.R. Denton, N.W. Ashcroft, Phys. Rev. A 43 (1991) 3161.
[30] S. Mukerjee, S. Srinivasan, M.P. Soriaga, J. Electrochem. Soc. 142 (1995) 1409.
[31] S. Mukerjee, S. Srinivasan, M.P. Soriaga, J. Mcbreen, J. Phys. Chem. 99 (1995) 4577.
[32] N. Furaya, S. Motoo, J. Electroanal. Chem. 98 (1979) 195.
[33] J.H. Kim, S.M. Choi, S.H. Nam, M.H. Seo, S.H. Choi, W.B. Kim, Appl. Catal. B 82 (2008) 89.
[34] M.-K. Min, J. Cho, K. Cho, H. Kim, Electrochim. Acta 45 (2000) 4211.
[35] R.B. Biniwale, N. Kariya, M. Ichikawa, Catal. Lett. 105 (2005) 83.
[36] A.H. Janowicz, R.G. Bergman, J. Am. Chem. Soc. 104 (1982) 352.
[37] J.K. Hoyano, W.A.G. Graham, J. Am. Chem. Soc. 104 (1982) 3722.